WATER RESOURCES RESEARCH, VOL. 49, 1–14, doi:10.1002/wrcr.20136, 2013

A reduced-order model for groundwater flow equation with random hydraulic conductivity: Application to Monte Carlo methods

Damiano Pasetto,[1] Mario Putti,[1] and William W-G. Yeh[2]

Received 24 August 2012; revised 30 December 2012; accepted 8 February 2013.

[1] We present a model-order reduction technique that overcomes the computational burden associated with the application of Monte Carlo methods to the solution of the groundwater flow equation with random hydraulic conductivity. The method is based on the Galerkin projection of the high-dimensional model equations onto a subspace, approximated by a small number of pseudo-optimally chosen basis functions (principal components). To obtain an efficient reduced-order model, we develop an offline algorithm for the computation of the parameter-independent principal components. Our algorithm combines a greedy algorithm for the snapshot selection in the parameter space and an optimal distribution of the snapshots in time. Moreover, we introduce a residual-based estimation of the error associated with the reduced model. This estimation allows a considerable reduction of the number of full system model solutions required for the computation of principal components. We demonstrate the robustness of our methodology by way of numerical examples, comparing the empirical statistics of the ensemble of the numerical solutions obtained using the traditional Monte Carlo method and our reduced model. The numerical results show that our methodology significantly reduces the computational requirements (CPU time and storage) for the solution of the Monte Carlo simulation, ensuring a good approximation of the mean and variance of the head. The analysis of the empirical probability density functions at the observation wells suggests that our reduced model produces good results and is most accurate in the regions with large drawdown.

Citation: Pasetto, D., M. Putti, and W. W-G. Yeh (2013), A reduced-order model for groundwater flow equation with random hydraulic conductivity: Application to Monte Carlo methods, *Water Resour. Res.*, *49*, doi:10.1002/wrcr.20136.

1. Introduction

[2] The physical description of groundwater flow in saturated porous media is derived from the solution of a parabolic partial differential equation. The application of this simple mathematical model to real hydrological systems depends on several parameters, such as the initial and boundary conditions, the forcing terms, and the aquifer properties, i.e., the hydraulic conductivity and the specific storage. In large aquifers, the heterogeneity of the soil is usually modeled by subdividing the aquifer into a number of zones, based on the geological formations of the aquifer. Then, in the classical deterministic approach, the calibration of the numerical model is usually achieved by solving an inverse problem [*Yeh*, 1986; *Oliver and Chen*, 2011], where the zonal parameter values are estimated by minimizing the discrepancies between the model output and observations. Because of the presence of measurement errors as well as the complexity and heterogeneity of the real system, convergence to the correct parameter values is not always guaranteed. The uncertainty of model parameters is taken into account in the probabilistic approach [*Dagan*, 1982], where the stochastic partial differential equation for the groundwater flow governs the evolution in time of the entire probability density function (PDF) of the head. This probabilistic approach is used in many applications, such as in a framework for forecasting and risk assessment, since it allows the quantification of the uncertainties in model predictions

[3] The solution of a stochastic groundwater flow problem is achieved by way of numerical techniques such as Monte Carlo (MC) methods [*Robert and Casella*, 2010; *Zhang et al*., 2010], moment differential equations [*Guadagnini and Neuman*, 1999], and polynomial chaos expansion [*Ghanem and Spanos*, 1991; *Li and Zhang*, 2007]. MC methods are widely used, as they can be implemented easily using the deterministic numerical solvers and give an approximation of the complete PDF of the head. MC methods provide the foundation for data assimilation techniques such as the ensemble Kalman filter [*Chen and Zhang*, 2006] and particle filters [*Pasetto et al*., 2012], and are used for the solution of inverse problems [*Hendricks Franssen et al*., 2009]. The main drawback of MC methods is that the empirical distribution converges slowly to the real probability distribution, such that many MC realizations are necessary to obtain accurate results. Since each MC realization

[1]Department of Mathematics, University of Padua, Padua, Italy.
[2]Department of Civil and Environmental Engineering, University of California, Los Angeles, California, USA.

Corresponding author: D. Pasetto, Department of Mathematics, University of Padua, I-35122 Padua, Italy. (damiano.pasetto@studenti.unipd.it)

0043-1397/13/10.1002/wrcr.20136

corresponds to a solution of the deterministic partial differential equation, this procedure is computationally expensive and even infeasible in high-dimensional models.

[4] In this paper we propose an efficient MC method for the solution of the transient groundwater flow equation with stochastic hydraulic conductivity. The idea is to reduce the computational requirements (CPU time and storage) associated with each single solution of the partial differential equation and, consequently, improve the efficiency of the MC method. With this purpose, we apply the proper orthogonal decomposition (POD) to the groundwater flow equation. The POD is a model-order reduction technique based on the selection of a small number of orthonormal basis functions (principal components) that span the spatial variability of the solutions. In this way the head is approximated by a linear combination of these basis functions, and, using a Galerkin projection, the dimension of the problem is reduced by several orders of magnitude [*Kunisch and Volkwein*, 2001]. Several applications of the POD to the groundwater flow problem have been reported in the literature. *Vermeulen et al*. [2004] applied the Galerkin projection and the state-space projection to a three-dimensional groundwater model with pumping. *McPhee and Yeh* [2008] demonstrated that the reduced model is able to reproduce the sensitivities of head with respect to pumping and directly embedded the reduced model in the constraint set of an optimization model for groundwater management. *Pasetto et al*. [2011] investigated the applicability of POD to a steady-state groundwater flow equation with randomly distributed recharge. *Siade et al*. [2012] used the POD to overcome the computational burden associated with the estimation of the hydraulic conductivity with the quasi-linearization method combined with quadratic programming. Using the concept of POD, *Baú* [2012] developed a stochastic groundwater flow-reduced model, which was used for parameter uncertainty analysis in connection with a multiobjective groundwater management problem.

[5] The computation of the principal components is the most important step in the construction of the reduced model. On one hand, to avoid large errors in the reduced model solution, we need a sufficient number of principal components to capture the dominating characteristics of the original full system model (FSM) in the reduced space. On the other hand, the number of principal components determines the dimension of the reduced model and, consequently, the computational time required to solve the reduced model. The snapshots technique is often used for the computation of the principal components associated with one particular model solution. *Siade et al*. [2010] introduced a methodology for the computation of optimal times for the selection of snapshots in such a way that the resulting principal components account for the maximal variance of the solution. This methodology is very efficient, as it requires only two runs of the FSM to select the optimal snapshots.

[6] In our application, the randomness of the hydraulic conductivity represents an additional source of variability in the space of the solutions. In theory, to obtain accurate reduced models, we should compute different principal components for each sample of the hydraulic conductivity [*Vermeulen et al*., 2004]. However, as the computation of the principal components requires the solution of the original FSM, the construction of a different reduced model for each MC realization would defeat the purpose of model reduction. A different approach is based on the idea that, if two realizations of hydraulic conductivity are statistically indistinguishable, a single set of principal components can be used for the construction of two reduced models (RMs). Moreover, we can argue that if the principal components are collected from appropriately chosen hydraulic conductivity values, then we can obtain a unique set of principal components that cover the entire parameter space.

[7] Heuristic methods, such as the greedy algorithm [*Grepl and Patera*, 2005], have been developed to select the snapshots in the parameter space. The goal is to choose a set of parameter values and, in an offline setting, improve the set of principal components until the solutions of the reduced model satisfy a validation condition. For this purpose, *Grepl and Patera* [2005] proposed an a posteriori error estimation based on the norm of the residual in which the computation of the residual does not involve the solution of the original FSM. We note that the "error" is defined as the difference between the FSM solution and the reduced model solution, while the "residual" is the vector obtained by substituting the reduced model solution into the FSM. Several examples of the use of residual norms to estimate the error norm are presented in the literature [*Grepl and Patera*, 2005; *Rovas et al*., 2006; *Haasdonk and Ohlberger*, 2011; *Hasenauer et al*., 2012]. Note that, for linear equations, error and residual norms are related by a scaling constant, which is difficult to evaluate [*Grepl and Patera*, 2005]. Hence, the main drawback in the application of the greedy algorithm with the validation condition based on a posteriori error estimation is that the norm of the residual can be much larger than that of the error, causing an overestimation of the error. This results in an inefficient reduced model in which the number of principal components is unnecessarily larger than the one actually needed to obtain the desired accuracy [*Hasenauer et al*., 2012]. An approach to resolve this problem is proposed by *Hinze and Kunkei* [2012], who applied the greedy algorithm to a nonlinear model with a one-dimensional parameter space and presented a practical way to estimate the reduced model error. They computed a scaling factor between the norm of the error and the norm of the residual for the realizations where the FSM solution is available and then linearly interpolated these values in the parameter space to compute a scaled residual for all the reduced model solutions.

[8] In this study, we present a new methodology for the computation of the principal components that combines the optimal snapshots selection in time of *Siade et al*. [2010] with the greedy algorithm of *Grepl and Patera* [2005] for the selection of snapshots in the parameter space. We improve the efficiency of the proposed approach by using the scaled reduced model residual to estimate the error, extending the approach of *Hinze and Kunkei* [2012] to a parameter space of general dimension and nonlinear interpolation. Hence, the scaling factor needed to relate error and residual norms is calculated "exactly" for those snapshots for which the FSM solution is available, while for the remaining runs it is interpolated from the "exact" values. The resulting algorithm for the offline process guarantees an efficient computation of the principal components. The unique set of principal components thus obtained is sufficient

to cover the variability of the head in both the parameter space and time domain. Additionally, our approach minimizes the number of FSM runs needed for the computation of snapshots. The application of the reduced model to the MC method is then straightforward. The reduced model not only dramatically reduces the computational requirements associated with each system solution but also permits a faster evaluation of the ensemble statistics.

[9] We use two numerical examples to demonstrate the validity and applicability of our proposed methodology: a one-dimensional synthetic test case and a two-dimensional model of the Oristano aquifer, in Italy. The accuracy of the reduced model results is assessed by way of a comparison with the standard MC solution in terms of ensemble mean and variance on the domain and PDF of the head at a number of observation wells.

2. Problem Setting

[10] We consider the governing equation describing a three-dimensional groundwater flow for a confined, anisotropic aquifer with pumping [*Bear*, 1979]:

$$S_s \frac{\partial h(\mathbf{x},t)}{\partial t} - \nabla \cdot (\mathbf{K} \nabla h(\mathbf{x},t)) = q(t), \quad \mathbf{x} \in \Omega \subset \mathbb{R}^3, \quad t \in [0, T_F], \tag{1}$$

where Ω is the domain of the aquifer, T_F is the final time [T], $\mathbf{x}$ is the vector of coordinates (x, y, z), h is the head [L], S_s is the specific storage [L^{-1}], q is the specific volumetric pumping rate [T^{-1}], and $\mathbf{K}$ is the hydraulic conductivity tensor:

$$\mathbf{K} = \begin{bmatrix} K_x & 0 & 0 \\ 0 & K_y & 0 \\ 0 & 0 & K_z \end{bmatrix},$$

with $K_x = K_y = K$ [LT^{-1}]. The initial and boundary conditions are

$$\begin{cases} h(\mathbf{x},0) = h_0(\mathbf{x}), & \mathbf{x} \in \Omega, \\ h(\mathbf{x},t) = h_D(\mathbf{x},t), & \mathbf{x} \in \Gamma_D \subset \partial\Omega, \\ -\mathbf{K}\nabla h(\mathbf{x},t) \cdot \mathbf{n}(\mathbf{x}) = q_N(\mathbf{x},t), & \mathbf{x} \in \Gamma_N \subset \partial\Omega, \end{cases}$$

where Γ_D and Γ_N are the Dirichlet and Neumann boundaries, respectively; h_0, h_D, and q_N are known functions; and $\mathbf{n}$ is the normal vector at the boundary. In the following, we consider a heterogeneous horizontal hydraulic conductivity, $K(\mathbf{x})$, while the other aquifer parameters are homogeneous. We model the heterogeneity of K by subdividing the domain Ω into n_z zones, $\Omega_1, \ldots, \Omega_{n_z}$, such that

$$\bigcup_{i=1}^{n_z} \Omega_i = \Omega, \quad \text{and} \quad \Omega_i \cap \Omega_j = \varnothing \text{ if } i \neq j,$$

and the hydraulic conductivity $K(\mathbf{x})$ is constant in each zone, with values $K_1, \ldots, K_{n_z}$ in $\Omega_1, \ldots, \Omega_{n_z}$, respectively. We indicate with $\mathbf{k}$ the vector of the n_z zonal values of conductivity, $\mathbf{k} = \{K_1, \ldots, K_{n_z}\}$. Here, we use zonation to parameterize the hydraulic conductivity into a number of zones, a method commonly adopted by groundwater practitioners. Additionally, in each zone, we know the upper bound and lower bound of the parameter. Further study is needed to extend the present work to a randomly distributed hydraulic conductivity field.

[11] Without loss of generality, we solve equation (1) for the drawdown s, defined as the difference between the head (h) resulting from pumping and the initial head (H), i.e., $s = H - h$. The initial and boundary conditions for the drawdown are $s_0 = 0$, $s_D = 0$, and $q_N = 0$. We will assume that the pumping rate is constant in time, a common practice for pumping tests. The proposed methodology also applies to a time-varying pumping rate. However, if more than one pumping well is present and the pumping rate varies with time, it is necessary to consider the response of each pumping well separately and then apply the principle of superposition.

[12] The solution of equation (1) is achieved numerically, e.g., via finite elements, finite differences, or finite volumes. A refined spatial discretization of the domain Ω, characterized by n_{nd} degrees of freedom (mesh nodes or cells), results in a high-dimensional linear system of ordinary differential equations (ODEs), written as

$$\mathbf{B}\frac{\partial \mathbf{s}(t,\mathbf{k})}{\partial t} + \mathbf{A}(\mathbf{k})\mathbf{s}(t,\mathbf{k}) = \mathbf{q}, \quad t \in [0, T_F], \tag{2}$$

where $\mathbf{A}$ (stiffness matrix) and $\mathbf{B}$ (mass matrix) are positive definite, symmetric, and sparse matrices of dimension $n_{nd} \times n_{nd}$, while $\mathbf{s}$ and $\mathbf{q}$ are the vectors of nodal drawdown and source/sinks, respectively. In particular, focusing on the linear finite element method with obvious adjustments for other discretizations, the stiffness matrix can be written as a linear combination of parameter-independent matrices $\mathbf{A}_i$:

$$\mathbf{A}(\mathbf{k}) = \mathbf{A}(K_1, \ldots, K_{n_z}) = \sum_{i=1}^{n_z} K_i \mathbf{A}_i. \tag{3}$$

[13] The components of each matrix $\mathbf{A}_i$ are evaluated using unit conductivity over the portion of the domain encompassing the i^{th} zone, i.e.,

$$(\mathbf{A}_i)_{rs} = \int_{\Omega_i} \nabla\varphi_r \cdot \nabla\varphi_s \mathrm{d}\Omega,$$

where φ_r and φ_s are the piecewise-linear basis functions used in our finite element approach. An equation similar to equation (3) also can be derived for the case of finite difference or finite volume schemes, where harmonic means of the conductivity values are used.

[14] The solution in time of equation (2) is achieved with a backward difference approximation, with variable time step length $\Delta t_l = t_l - t_{l-1}$, leading to the following linear system of algebraic equations:

$$\left(\frac{1}{\Delta t_l}\mathbf{B} + \mathbf{A}(\mathbf{k})\right)\mathbf{s}(t_l,\mathbf{k}) = \frac{1}{\Delta t_l}\mathbf{B}\,\mathbf{s}(t_{l-1},\mathbf{k}) + \mathbf{q}, \quad l = 1, \ldots, l_F. \tag{4}$$

[15] We term equation (4) as the full system model (FSM).

[16] The unknown hydraulic conductivity values K_i are modeled as random variables with a given probability

distribution [*Dagan*, 1982]. In this paper we consider that K_i values are uniformly distributed random variables:

$$K_i \sim U\left(K_i^{\min}, K_i^{\max}\right),$$

where $K_i^{\min}$ and $K_i^{\max}$ are the lower bound and upper bound, respectively, of K_i. We use a uniform distribution since the upper bound and lower bound of the hydraulic conductivity in each zone are usually available during model calibration. However, our proposed methodology applies to other probability distributions as well. MC methods can be used to approximate the temporal evolution of the PDF of the head, h, by solving equation (4) for several independent samples of the hydraulic conductivity $\mathbf{k}$. Let $\mathcal{L} = \left\{\mathbf{k}^1, \ldots, \mathbf{k}^{n_{\text{ens}}}\right\}$ be the ensemble of MC realizations of hydraulic conductivity, where n_{ens} is the number of samples. The PDF of the drawdown at time t_l is then approximated by the empirical distribution of the ensemble of solutions $\mathbf{s}\left(t_l, \mathbf{k}^1\right), \ldots, \mathbf{s}\left(t_l, \mathbf{k}^{n_{\text{ens}}}\right)$. MC methods are more accurate when a large number n_{ens} of FSM solutions are used; this procedure is computationally expensive and impractical for high-dimensional models (large n_{nd}).

3. Reduced-Order Methods

[17] Model reduction methods can decrease the computational cost associated with the solution of equation (4). The idea of Galerkin model reduction techniques [*Kunisch and Volkwein*, 2001] is to compute an approximated drawdown, $\tilde{\mathbf{s}}(t_l, \mathbf{k}^j)$, using a suitable linear combination of a small number of basis functions (also called principal components), $\mathbf{p}_1, \ldots, \mathbf{p}_{n_{pc}}$, where $\mathbf{p}_i$ is a n_{nd}-dimensional vector and n_{pc} is the number of principal components used in the reduction. Indicating with $\mathbf{P}$ the $n_{nd} \times n_{pc}$ matrix whose columns are $\mathbf{p}_i, \ldots, \mathbf{p}_{n_{pc}}$, we arrive at

$$\mathbf{s}\left(t_l, \mathbf{k}^j\right) \approx \tilde{\mathbf{s}}\left(t_l, \mathbf{k}^j\right) = \mathbf{P}\,\mathbf{a}\left(t_l, \mathbf{k}^j\right). \tag{5}$$

[18] The n_{pc}-dimensional vector $\mathbf{a}$ is the solution of the reduced-order equation obtained substituting $\mathbf{s}$ with $\tilde{\mathbf{s}}$ in equation (4) and applying the Galerkin projection with respect to $\mathbf{P}$:

$$\left(\frac{1}{\Delta t_l}\tilde{\mathbf{B}} + \tilde{\mathbf{A}}\left(\mathbf{k}^j\right)\right)\mathbf{a}\left(t_l, \mathbf{k}^j\right) = \frac{1}{\Delta t_l}\tilde{\mathbf{B}}\,\mathbf{a}\left(t_{l-1}, \mathbf{k}^j\right) + \tilde{\mathbf{q}}, \tag{6}$$

where $\tilde{\mathbf{A}}(\mathbf{k}^j) = \mathbf{P}^T\mathbf{A}(\mathbf{k}^j)\mathbf{P}$, $\tilde{\mathbf{B}} = \mathbf{P}^T\mathbf{B}\mathbf{P}$, and $\tilde{\mathbf{q}} = \mathbf{P}^T\mathbf{q}$. We refer to equation (6) as the reduced model (RM). Note that the matrix $\tilde{\mathbf{B}}$ is parameter independent, so it can be computed once and then stored. Due to the linear dependence of $\mathbf{A}$ on the hydraulic conductivity (equation (3)), the computation of $\tilde{\mathbf{A}}$ also does not depend on the original high dimension n_{nd}:

$$\tilde{\mathbf{A}}(\mathbf{k}) = \sum_{i=1}^{n_z} K_i\mathbf{P}^T\mathbf{A}_i\mathbf{P} = \sum_{i=1}^{n_z} K_i\tilde{\mathbf{A}}_i, \tag{7}$$

where the matrices $\tilde{\mathbf{A}}_i$ are parameter-independent matrices in the reduced dimension. In this way, the assembly and the solution of RM (equation (6)) are performed only in the reduced dimension n_{pc}.

[19] An RM is accurate if the error $\mathbf{e}(t_l, \mathbf{k}^j)$ between the FSM and RM solutions

$$\mathbf{e}\left(t_l, \mathbf{k}^j\right) = \mathbf{s}\left(t_l, \mathbf{k}^j\right) - \tilde{\mathbf{s}}\left(t_l, \mathbf{k}^j\right) \tag{8}$$

is small (in norm). The error associated with the RM is estimated a posteriori using the computation of the residual vector $\mathbf{r}(t_l, \mathbf{k}^j)$ obtained by replacing $\mathbf{s}$ with $\tilde{\mathbf{s}}$ in equation (4) [*Grepl and Patera*, 2005; *Rovas et al.*, 2006; *Hasenauer et al.*, 2012]:

$$\begin{aligned}\mathbf{r}\left(t_l, \mathbf{k}^j\right) = &-\left(\frac{1}{\Delta t_l}\mathbf{B} + \mathbf{A}\left(\mathbf{k}^j\right)\right)\mathbf{P}\,\mathbf{a}\left(t_l, \mathbf{k}^j\right) \\ &+ \frac{1}{\Delta t_l}\mathbf{B}\mathbf{P}\quad \mathbf{a}\left(t_{l-1}, \mathbf{k}^j\right) + \mathbf{q}.\end{aligned} \tag{9}$$

[20] The error is related to the residual by the following equation:

$$\mathbf{r}\left(t_l, \mathbf{k}^j\right) = \left(\frac{1}{\Delta t_l}\mathbf{B} + \mathbf{A}\left(\mathbf{k}^j\right)\right)\mathbf{e}\left(t_l, \mathbf{k}^j\right) - \frac{1}{\Delta t_l}\mathbf{B}\,\mathbf{e}\left(t_{l-1}, \mathbf{k}^j\right). \tag{10}$$

[21] Equations (9) and (10) reveal two important properties of the residual: (i) the residual is computed without knowing the corresponding FSM solution and (ii) the residual is zero when the error is zero. Moreover, *Haasdonk and Ohlberger* [2011] demonstrated the following a posteriori error estimate:

$$\begin{aligned}\left\|\mathbf{e}\left(t_l, \mathbf{k}^j\right)\right\|_2 &\le C\left(\mathbf{k}^j\right)\left(\left\|\mathbf{r}\left(t_0, \mathbf{k}^j\right)\right\|_2 + \int_0^{t_l}\left\|\mathbf{r}\left(\tau, \mathbf{k}^j\right)\right\|_2 \mathrm{d}\tau\right) \\ &= R\left(t_l, \mathbf{k}^j\right),\end{aligned} \tag{11}$$

where

$$\|\mathbf{e}\|_2 = \sqrt{\sum_{i=1}^{n_{nd}} e_i^2}$$

and $C(\mathbf{k}^j)$ is a constant that can be approximated by the value 1 for our particular model [*Haasdonk and Ohlberger*, 2011]. We note that $\mathbf{r}(t_l, \mathbf{k}^j)$ is the residual vector, while $R(t_l, \mathbf{k}^j)$ is the estimation of the error norm based on the time-integrated norm of the residual. We can compute $R(t_l, \mathbf{k}^j)$ in the reduced dimension n_{pc} in the following manner:

$$\begin{aligned}\left\|\mathrm{r}\left(t_l, \mathbf{k}^j\right)\right\|_2 = &\left(\mathbf{a}_l^j\right)^T\mathbf{P}^T\left(\frac{1}{\left(\Delta t_l\right)^2}\mathbf{B}^T\mathbf{B} + \frac{2}{\Delta t_l}\mathbf{B}^T\mathbf{A}^j + \left(\mathbf{A}^j\right)^T\mathbf{A}^j\right)\mathbf{P}\ \mathbf{a}_l^j \\ &- 2\left(\mathbf{a}_l^j\right)^T\mathbf{P}^T\left(\frac{1}{\left(\Delta t_l\right)^2}\mathbf{B}^T\mathbf{B} + \frac{1}{\Delta t_l}\left(\mathbf{A}^j\right)^T\mathbf{B}\right)\mathbf{P}\ \mathbf{a}_{l-1}^j \\ &- 2\left(\mathbf{a}_l^j\right)^T\mathbf{P}^T\left(\frac{1}{\left(\Delta t_l\right)^2}\mathbf{B}^T + \left(\mathbf{A}^j\right)^T\right)\mathbf{q} \\ &+ \left(\mathbf{a}_{l-1}^j\right)^T\mathbf{P}^T\left(\frac{1}{\left(\Delta t_l\right)^2}\mathbf{B}^T\mathbf{B}\right)\mathbf{P}\ \mathbf{a}_{l-1}^j \\ &+ 2\left(\mathbf{a}_{l-1}^j\right)^T\mathbf{P}^T\left(\frac{1}{\Delta t_l})\mathbf{B}^T\right)\mathbf{q} \\ &+ \mathbf{q}^T\mathbf{q},\end{aligned} \tag{12}$$

where the matrices $\mathbf{P}^T\mathbf{B}^T\mathbf{B}\mathbf{P}$, $\mathbf{P}^T\left(\mathbf{A}^j\right)^T\mathbf{B}\mathbf{P}$, $\mathbf{P}^T\left(\mathbf{A}^j\right)^T\mathbf{A}^j\mathbf{P}$, the vectors $\mathbf{P}^T\mathbf{B}^T\mathbf{q}$, $\mathbf{P}^T\left(\mathbf{A}^j\right)^T\mathbf{q}$, and the scalar $\mathbf{q}^T\mathbf{q}$ can be computed offline (a procedure similar to the one used in equation (7) applies for the parameter-dependent quantities). Note that, to simplify the notation, in the previous equation the time and parameter dependences are shown with the indices l and j, respectively.

[22] In the following we present an efficient algorithm to compute the principal components $\mathbf{p}_i$. We search for principal components that are time- and parameter independent, and that can be applied to the construction of RM associated with each realization of hydraulic conductivity in $\mathcal{L}$. In this way, the expensive computation of the principal components is performed only once, in an offline setting, i.e., before the application of the RM to the MC simulation. We select a set of hydraulic conductivity values $\mathcal{K}$, $\mathcal{K} = \left\{\hat{\mathbf{k}}^1, \ldots, \hat{\mathbf{k}}^{n_k}\right\}$, to validate the RM accuracy (the validation set). The set $\mathcal{K}$ can be different from the set $\mathcal{L}$; thus, we use the symbol "$\hat{}$" to distinguish between the realizations in $\mathcal{K}$, used for the offline process, and the random realizations in $\mathcal{L}$, used in the MC simulation. We start from a reduced model of dimension one and compute the RM solution for all realizations in the validation set $\mathcal{K}$. Then, we increase the number of principal components until the error associated with the RM solution is less than a given tolerance for all realizations in $\mathcal{K}$.

3.1. Optimal Snapshots Selection in Time

[23] The reduced model is initialized considering the first realization in $\mathcal{K}$, $\hat{\mathbf{k}}^1$. Our choice is to select $\hat{\mathbf{k}}^1$ as the realization with the mean value of the conductivity in each zone. In this way the reduced model reproduces the average response of the system. Then, the principal components are computed based on the transient FSM solution for $\hat{\mathbf{k}}^1$, to capture the dominating characteristics of the solution in time.

[24] Given a realization of the hydraulic conductivity $\mathbf{k}$ and given a fixed number n_{pc} of basis functions for the reduced model, it is possible to compute an optimal set of time-independent principal components that minimizes the errors $\mathbf{e}(t_l, \mathbf{k})$, for $l = 1, \ldots, l_F$. The snapshots technique [*Vermeulen et al*., 2004] is a practical method developed for the computation of the principal components. This requires the storage of the FSM solution at specific times, $\hat{t}_1, \ldots, \hat{t}_{n_{sn}}$. The solution vectors obtained at these times are called snapshots and are indicated by $\mathbf{s}_{\hat{t}_1}, \ldots, \mathbf{s}_{\hat{t}_{n_{sn}}}$. Then, we apply the principal component analysis (PCA) on the set of the snapshots to identify the optimal basis functions to be included to approximate the snapshots. In principle, to completely characterize the FSM solution, we should store a snapshot for each time step. This is not feasible in high-dimensional systems, but unnecessary since very little new information will be provided if snapshots are taken close to each other in time where the rate of change in drawdown is small.

[25] *Siade et al*. [2010] suggested a general procedure for selecting optimal snapshot times for the groundwater equation (equation (1)). Let T_s be the time at which the solution $\mathbf{s}(T_S, \mathbf{k})$ approximately reaches a steady state. This can be computed by solving the FSM equation (4) with a termination condition:

$$\frac{\|\mathbf{s}(t_l, \mathbf{k}) - \mathbf{s}(t_{l-1}, \mathbf{k})\|_2}{\|\mathbf{s}(t_l, \mathbf{k})\|_2} \leq \tau_S,$$

with the tolerance τ_S sufficiently small (e.g., $\tau_S = 10^{-3}$) or, when appropriate, with other simple approximations based, e.g., on the Theis equation. The optimal snapshot times $\hat{t}_i$ are then located along an exponential function:

$$t(u) = \frac{T_S}{0.9}(\beta e^{\alpha u} + \gamma), \quad u \geq 0, \tag{13}$$

where α, β, and γ are computed using the results presented in *Siade et al*. [2010].

[26] Finally, as we are interested in the solution of equation (1) in time interval $[0, T_F]$, we choose $\hat{t}_1 = \Delta t_1$ and $\hat{t}_{n_{sn}} = T_F$. Let u_1 and $u_{n_{sn}}$ be such that $t(u_1) = \hat{t}_1$ and $t(u_{n_{sn}}) = \hat{t}_{n_{sn}}$, respectively, using equation (13). The other snapshot times are computed using equation (13) on equally spaced values of u, with step $\Delta u = (u_{n_{sn}} - u_1)/(n_{ns} - 1)$:

$$(u_1, \ldots, u_i = u_{i-1} + \Delta u, \ldots, u_{n_{sn}}).$$

[27] The appealing feature of this method is the possibility of computing n_{sn} quasi-optimal snapshots with only two FSM runs. A PCA is applied on the snapshots, and the corresponding principal components $\mathbf{p}_1^j, \ldots, \mathbf{p}_{n_{sn}}^j$ are stored (the index j means that the principal components are computed from the realization $\mathbf{k}^j$). Moreover, as we solve the FSM to get the snapshots, we can store the FSM solution at the output times and then compute the error associated with the RM solution at these times. If the error is above a tolerance value τ_e, then the RM can be improved adding a new principal component. Note that the principal components are ordered in such a way that, if the desired dimension of the RM is n_{pc}, then the RM constructed with the first n_{pc} principal components, $\mathbf{p}_1^j, \ldots, \mathbf{p}_{n_{pc}}^j$, is the one that minimizes the error. For this reason, the best way to improve the RM is to add the first unused principal component to the set $\mathbf{p}_1^j, \ldots, \mathbf{p}_{n_{sn}}^j$. To summarize, we use Algorithm 1, shown in Appendix A, to initialize the RM.

3.2. Snapshot Selection in the Parameter Space

[28] The greedy algorithm is a heuristic method used to determine which parameter values in $\mathcal{K}$ are to be selected for generating the snapshots without applying Algorithm 1, i.e., the FSM, to each realization $\hat{\mathbf{k}}^i$. The main idea is to compute the new snapshots for the realization in $\mathcal{K}$ where the RM solution gives the worst approximation of the FSM solution. In this way we improve the RM by including the basis functions that were not previously considered. Since the FSM solution is not available for all realizations in $\mathcal{K}$, we use the estimation of error based on the residual (equation (11)) to determine whether the RM solution is accurate.

[29] The matrix of the principal components $\mathbf{P}$ is initialized as described in the previous section. Then, we compute the RM solution and the norm of the corresponding residual for each realization in $\mathcal{K}$. If the maximum norm of the residual is above a specified tolerance value τ_e, we compute the FSM corresponding to the realization with the maximum norm of the residual in agreement with the greedy algorithm. The matrix of the principal components is updated using Algorithm 1. We repeat these operations until the maximum norm of the residual is smaller than a specified tolerance value for all realizations in $\mathcal{K}$.

[30] We let $\mathcal{K}^* = \{\hat{\mathbf{k}}^{*1}, \ldots, \hat{\mathbf{k}}^{*n_{gr}}\}$, ($\mathcal{K}^* \subset \mathcal{K}$), be the set of the n_{gr} parameter values selected from the first n_{gr} iterations of the greedy algorithm: in other words, at the n_{gr}^{th} iteration of the greedy algorithm, $\hat{\mathbf{k}}^{*n_{gr}}$ satisfies

$$\hat{\mathbf{k}}^{*n_{gr}} = \arg\max_{\hat{\mathbf{k}}^i \in \mathcal{K}} R\left(T_F, \hat{\mathbf{k}}^i\right). \tag{14}$$

[31] Note that we use the symbol "*" to indicate the realizations in $\mathcal{K}$ for which we compute the snapshots. For each realization $\hat{\mathbf{k}}^{*j}$, we select snapshots in time and collect the corresponding principal components $\mathbf{p}^{*j}$ as described in Algorithm 1. To ensure the orthogonality of matrix $\mathbf{P}$, the new principal components are orthonormalized with respect to the columns of $\mathbf{P}$ and possible redundant principal components are discarded. Moreover, at each modification of the principal components, it is convenient to check whether the error still satisfies the validation condition for all the realizations in $\mathcal{K}^*$. If the condition is not satisfied, more principal components are selected from the realization with the maximum error, without any additional FSM run.

[32] Since the norm of the residual $R(T_F, \hat{\mathbf{k}}^i)$ can be much larger than the norm of the error, using equation (11) in the greedy algorithm may select more principal components than necessary in order to satisfy the desired accuracy [*Hasenauer*, 2012]. Following the suggestion of *Hinze and Kunkei* [2012], we scale the norm of the residual $R(T_F, \hat{\mathbf{k}}^i)$ to better estimate the error. We note that for all the realizations in $\mathcal{K}^*$ we know both the error and the residual. Then for these realizations, we compute an exact scaling factor ρ^{*j} such that

$$\rho^{*j} = \frac{\|\mathbf{e}\left(T_F, \hat{\mathbf{k}}^{*j}\right)\|_2}{R\left(T_F, \hat{\mathbf{k}}^{*j}\right)}, \quad \forall\ \hat{\mathbf{k}}^{*j} \in \mathcal{K}^*. \tag{15}$$

[33] For the other realizations in $\mathcal{K}$, we approximate the scaling factor ρ^i associated with $\hat{\mathbf{k}}^i$, interpolating the values ρ^{*j} with respect to the hydraulic conductivity. For this purpose, we need to introduce a metric in the parameter space that relates the change in drawdown to the change in hydraulic conductivity. We consider the following distance $d^{i,j}$ between $\hat{\mathbf{k}}^i$ and realization $\hat{\mathbf{k}}^{*j}$ in $\mathcal{K}^*$:

$$d^{i,j} = \sqrt{\sum_{m=1}^{n_z} \left(\frac{1}{\hat{K}_m^i} - \frac{1}{\hat{K}_m^{*j}}\right)^2}, \quad j = 1, \ldots, n_{gr},$$

where the inverse values of $\hat{K}_m^i$ are used to take into account the inverse relation between drawdown and hydraulic conductivity. Let $\hat{\mathbf{k}}^{*r}$ and $\hat{\mathbf{k}}^{*s}$ be the two conductivity values in $\mathcal{K}^*$ closest to $\hat{\mathbf{k}}^i$ with associated distances $d^{i,r}$, $d^{i,s}$, and scaling factors ρ^{*r} and ρ^{*s}. We propose the following scaling function:

$$\rho^i = \begin{cases} \left|1 - (1-\rho^{*r})\exp\left(-\dfrac{d^{i,r}}{\lambda}\right)\right|, & \text{if } n_{gr} = 1. \\ \left|1 - (1-\rho^{*r})\exp\left(-\dfrac{d^{i,r}}{\lambda}\right) - (1-\rho^{*s})\exp\left(-\dfrac{d^{i,s}}{\lambda}\right) - \right. \\ \left. \quad (1 - 0.5(\rho^{*r}+\rho^{*s}))\exp\left(-\dfrac{d^{i,r}+d^{i,s}}{\lambda}\right)\right|, & \text{if } n_{gr} \geq 2. \end{cases} \tag{16}$$

[34] This scaling is defined such that, if the distances $d^{i,r}$ and $d^{i,s}$ are large, ρ^i is about 1 (no scaling): otherwise, ρ^i varies continuously between ρ^{*r}, ρ^{*s}, and $0.5(\rho^{*r} + \rho^{*s})$. The factor λ controls the shape of the scaling function. When $n_{gr} = 1$, large values of λ result in scaling factors ρ^i closer to ρ^{*r}, while small values result in scaling factors closer to 1.

[35] Let $\hat{R}\left(T_F, \hat{\mathbf{k}}^i\right)$ be the scaled residual

$$\hat{R}\left(T_F, \hat{\mathbf{k}}^i\right) = \rho^i R\left(T_F, \hat{\mathbf{k}}^i\right). \tag{17}$$

[36] We apply the greedy algorithm with the following modification of equation (14):

$$\hat{\mathbf{k}}^{*n_{gr}} = \arg\max_{\hat{\mathbf{k}}^i \in \mathcal{K}} \hat{R}\left(T_F, \hat{\mathbf{k}}^i\right). \tag{18}$$

[37] The resulting procedure is summarized in Algorithm 2 (shown in Appendix B).

[38] A crucial point in the application of Algorithm 2 is the choice of an adequate set $\mathcal{K}$, i.e., the set of realizations of hydraulic conductivity for the validation of the RM over the entire parameter space. A possible choice is to set $\mathcal{K} \subseteq \mathcal{L}$, i.e., to validate the RM directly on a subset of the preselected set of MC realizations. We prefer to explore another approach, to avoid the dependency of the offline algorithm to the random realizations. We note that (i) the RM is accurate when the parameter values are close to each other and (ii) in the offline stage we are interested in the validation of the RM for the worst parameter combinations. Therefore, we propose to select $\mathcal{K}$ as the set of all possible combinations of the upper bound, lower bound, and the mean of the hydraulic conductivity in all zones. If a different probability distribution describes the hydraulic conductivity, then the same choice is possible for $\mathcal{K}$, considering the tails (e.g., the first and the last 10 quantiles) and the median of the distribution instead of the upper bound, lower bound, and mean. With this approach the size of $\mathcal{K}$ increases rapidly with the number of zones, $n_k = 3^{n_{zn}}$, compromising the computational cost. However, Algorithm 2 still can be efficient because only the RM runs for all n_k realizations, while the FSM solution is computed only for a few realizations. If the number of combinations $3^{n_{zn}}$ far exceeds the number of realizations n_{ens}, then we still can apply the offline procedure directly on the set of realizations $\mathcal{L}$ used in the MC method.

3.3. Online: Monte Carlo and RM

[39] The online procedure consists of applying the RM to the MC method, i.e., the solution of equation (6) for all the realizations of hydraulic conductivity in $\mathcal{L}$. Then, the desired statistics (i.e., spatial mean, spatial variance, PDF at the output nodes) are computed from the ensemble of solutions $\tilde{\mathbf{s}}\left(t_i^{\text{out}}, \mathbf{k}^1\right), \ldots, \tilde{\mathbf{s}}\left(t_i^{\text{out}}, \mathbf{k}^{n_{\text{ens}}}\right)$ at the output times $t_1^{\text{out}}, \ldots, t_F^{\text{out}}$. The low dimension of the RM allows us to efficiently evaluate the ensemble statistics. As the matrix $\tilde{\mathbf{B}}$ and vector $\tilde{\mathbf{q}}$ are computed offline, the RM is assembled simply, using equation (7) to compute the matrix $\tilde{\mathbf{A}}$ (computational cost $O(n_{zn}\ n_{pc}^2)$). Then, equation (6) requires the solution of a linear system of dimension $n_{pc} \times n_{pc}$ for each time step. For calculating the statistics of the drawdown at the output time t_i^{out}, we let $\mu_{\tilde{\mathbf{s}}}\left(t_i^{\text{out}}\right)$ and $\mathbf{C}_{\tilde{\mathbf{s}}}\left(t_i^{\text{out}}\right)$

be the n_{nd}-dimensional vector of the mean and the $n_{nd} \times n_{nd}$ covariance matrix of the ensemble $\tilde{\mathbf{s}}(t_i^{\text{out}}, \mathbf{k}^j)$, respectively. These quantities are efficiently computed using equation (5) without the solution in the high-dimensional space:

$$\begin{aligned}\mu_{\tilde{\mathbf{s}}}(t_i^{\text{out}}) &= \frac{1}{n_{\text{ens}}}\sum_{j=1}^{n_{\text{ens}}}\tilde{\mathbf{s}}(t_i^{\text{out}}, \mathbf{k}^j)\\ &= \frac{1}{n_{\text{ens}}}\sum_{j=1}^{n_{\text{ens}}}\mathbf{P}\,\mathbf{a}(t_i^{\text{out}}, \mathbf{k}^j)\\ &= \mathbf{P}\frac{1}{n_{\text{ens}}}\sum_{j=1}^{n_{\text{ens}}}\mathbf{a}(t_i^{\text{out}}, \mathbf{k}^j)\\ &= \mathbf{P}\,\mu_{\mathbf{a}}(t_i^{\text{out}}),\end{aligned}$$

where $\mu_{\mathbf{a}}$ is the n_{pc}-dimensional vector of the mean values of the coefficient $\mathbf{a}$

$$\begin{aligned}\mathbf{C}_{\tilde{\mathbf{s}}}(t_i^{\text{out}}) &= \frac{1}{n_{\text{ens}}-1}\sum_{j=1}^{n_{\text{ens}}}\left(\tilde{\mathbf{s}}(t_i^{\text{out}}, \mathbf{k}^j) - \mu_{\tilde{\mathbf{s}}}(t_i^{\text{out}})\right)\left(\tilde{\mathbf{s}}(t_i^{\text{out}}, \mathbf{k}^j)\right.\\ &\quad\left.-\mu_{\tilde{\mathbf{s}}}(t_i^{\text{out}})\right)^T\\ &= \frac{1}{n_{\text{ens}}-1}\sum_{j=1}^{n_{\text{ens}}}\mathbf{P}\left(\mathbf{a}(t_i^{\text{out}}, \mathbf{k}^j) - \mu_{\mathbf{a}}(t_i^{\text{out}})\right)\left(\mathbf{a}(t_i^{\text{out}}, \mathbf{k}^j)\right.\\ &\quad\left.-\mu_{\mathbf{a}}(t_i^{\text{out}})\right)^T\mathbf{P}^T\\ &= \mathbf{P}\quad\mathbf{C}_{\mathbf{a}}(t_i^{\text{out}})\quad\mathbf{P}^T,\end{aligned}$$

where $\mathbf{C}_{\text{a}}$ is the $n_{pc} \times n_{pc}$ covariance matrix of the coefficient $\mathbf{a}$.

4. Numerical Results

4.1. One-Dimensional Model, TC1

[40] To validate our proposed methodology, we first consider the synthetic test case used by both *McPhee and Yeh* [2008] and *Siade et al*. [2012]. Figure 1 depicts a one-dimensional aquifer of length 100 m, with a pumping well located in the center and Dirichlet boundary conditions of 0 m. The thickness of the aquifer (b) is 1 m with a constant specific storage (S_s) of 1 m^{-1} so that in equation (1) the elastic storage represents the storage coefficient and the hydraulic conductivity tensor represents scalar transmissivity. The aquifer is subdivided into five zones, and the hydraulic conductivity is modeled as a uniformly distributed random variable in each zone, with lower bound $K_i^{\min} = 0.1$ m/d and upper bound $K_i^{\max} = 20$ m/d. We consider a pumping test with duration of 100 days ($T_F = 100$ d) with a constant pumping rate of $q = 10$ m^3/d. We name this test case TC1. The numerical simulation is performed with the program Sat2D [*Gambolati et al*., 1999], a finite element-based software for the simulation of saturated groundwater flow with a preconditioned conjugate gradient solver for the linear system arising from equation (4). The FSM consists of $n_{nd} = 303$ nodes (three lines of 101 nodes each). To take into account the random parameters, we apply the MC method using $n_{\text{ens}} = 10{,}000$ independent realizations of hydraulic conductivity. The ensemble-based statistics on the drawdown are computed and stored every 5 days, for a total of 21 output times. The numerical simulation of this simple scenario requires a CPU time of about 21 min, i.e., 0.13 s for each MC realization.

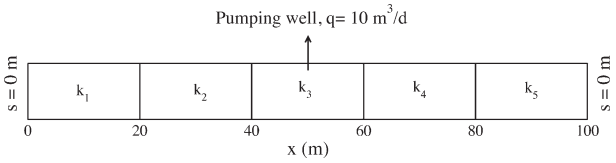

Figure 1. Sketch of the one-dimensional aquifer used for TC1.

[41] To improve the computational efficiency of the MC simulation, we apply our RM, using Algorithm 2 to compute the parameter-independent principal components. The set $\mathcal{K}$ consists of $3^5 = 243$ realizations of hydraulic conductivity. The tolerance on the average nodal error τ_e is set to 10^{-3} m while the value of λ for the computation of the scaling factors ρ^i (equation (16)) is set to 1000 m^2. For each $\mathcal{K}^*$realization, we store $n_{sn} = 15$ snapshots at the optimal times computed by equation (13) with the following values for the parameters [*Siade et al*., 2010]:

$$t(0) = 1.11 \times 10^{-7} T_s, \quad t(1) = T_s, \quad \gamma = -3.87 \times 10^{-6}.$$

[42] Table 1 shows the comparison of CPU times between the FSM and the RM for the MC simulation. It also shows the CPU time required for the offline and online calculations. The offline procedure for TC1 requires the computation of 24 FSM solutions (12 for the computation of the steady-state time T_s and 12 for the selection of the snapshots) and 3295 RM solutions, for a total CPU time of 14 s. The resulting RM has dimension $n_{pc} = 30$ (compared with $n_{nd} = 101$), which corresponds to a RM about 40 times faster than the FSM (0.3×10^{-2} s per realization).

[43] To demonstrate the accuracy and efficiency of Algorithm 2 with the modified greedy algorithm, Figure 2 reports the norm of the error $\|\mathbf{e}^i\|$, the norm of the residual R^i and the scaled norm of the residual $\hat{R}^i$ for all the realizations in $\mathcal{K}$. Figure 2a refers to the first iteration of the algorithm, when the snapshots are taken only from one realization (solid vertical line) and new snapshots are computed for the realization with maximum $\hat{R}^i$ (dotted vertical line). Figure 2b shows the last iteration. The horizontal line represents the error tolerance $\tau_e = 10^{-3}$. The continuous vertical lines indicate the realizations where the FSM solution is computed. We can see that, in the first iteration, the RM accurately approximates only the realization from which the snapshots are selected and is not parameter independent (because the error is above the tolerance value). Moreover, the scaled norm of the residual underestimates the norm of the error, which is actually closer to R^i. This is due to the fact that we are computing the scaling factors ρ^i,

Table 1. Comparison Between the FSM and RM CPU Times for the MC Simulation for TC1

			Time for One Iteration (s)	Total Time (s)
FSM	$n_{\text{ens}} = 10{,}000$	$n_{nd} = 303$	0.12	1279
RM online	$n_{\text{ens}} = 10{,}000$	$n_{pc} = 30$	0.35×10^{-2}	110
RM offline	$n_k = 243$	$n_{gr} = 12$		14
RM total				124

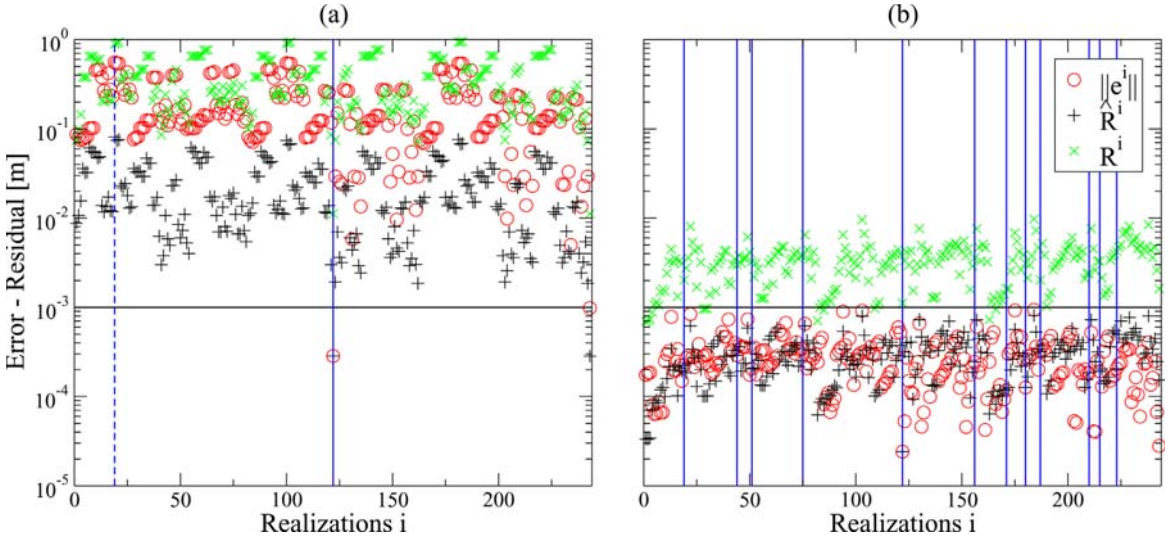

Figure 2. Norm of the error $\|\mathbf{e}\|$, scaled residual norm $\hat{R}$, and residual norm R associated with all realizations in $\mathcal{K}$ at the first and last iteration of the greedy algorithm in TC1. The continuous vertical blue lines indicate the realizations selected by the greedy algorithm for the computation of the snapshots. The dashed vertical blue line indicates the realization with the maximum scaled residual after the first iteration of the greedy algorithm. (a) First iteration and (b) last iteration.

using only one correct value ρ^*, and the large value chosen for λ imposes almost the same value of the scaling factor to all the realizations. Larger values of λ can cause a gross underestimation of the error, with the risk of falsely validating the RM when the real errors may still be very large. Figure 2b shows the results from the last iteration of Algorithm 2. In this case the RM is more accurate for all the parameter values in $\mathcal{K}$, as it consists of 30 principal components obtained from 12 FSM solutions. The scaled norm of the residual, $\hat{R}^i$, provides a good estimate of the norm of the errors, as both these values are below the required tolerance. In contrast, the norm of the residual, R^i, overestimates the error. This shows that if the validation condition is based only on the unscaled residual R^i, the greedy algorithm may proceed with the calculation of additional principal components that are unnecessary.

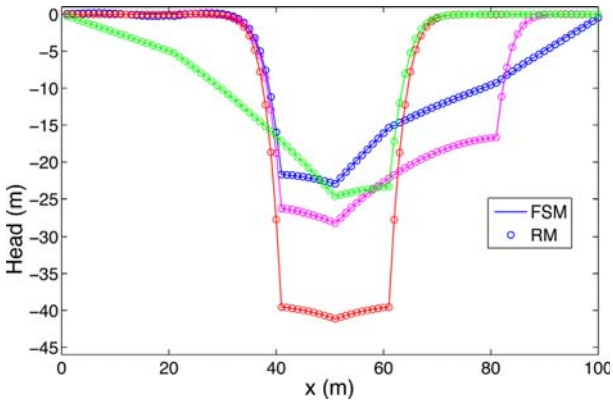

Figure 3. Comparison between four FSM solutions and the respective RM solutions for TC1.

[44] Figure 3 compares the FSM and the RM head for four realizations of the hydraulic conductivity in $\mathcal{K}$ at time T_F. Although the four FSM solutions exhibit very different profiles, the solutions obtained from the RM, utilizing the 30 parameter-independent principal components computed in the offline algorithm, are indistinguishable when compared with the FSM solutions.

[45] Finally, to demonstrate the applicability of the RM to MC simulations in TC1, we compare the ensemble statistics produced by the FSM and the RM solutions. For this purpose, we compute the FSM and the RM covariance matrices of the so-called augmented state, the vector of the nodal solutions $\mathbf{s}(t, \mathbf{k})$ augmented with the associated vector of the hydraulic conductivity $\mathbf{k}$. We indicate with $\mathbf{z}(t, \mathbf{k})$ the vector of the augmented state

$$\mathbf{z}(t, \mathbf{k}) = (z_1, \ldots, z_{n_{nd}+n_z}) = (s_1(t, \mathbf{k}), \ldots, s_{n_{nd}}(t, \mathbf{k}), k_1, \ldots, k_{n_z}).$$

[46] Figure 4 shows the matrix of the correlation coefficients associated with the augmented state of the system, computed with the FSM at the final time (T_F). Each element (i, j) of the correlation matrix is computed by the following equation:

$$\mathrm{Corr}\,(z_i, z_j) = \frac{\mathrm{Cov}\,(z_i, z_j)}{\sigma_{z_i}\sigma_{z_j}},$$

where Corr is the correlation, Cov is the covariance, and σ is the standard deviation. Figure 5 shows the errors between the correlation coefficients computed with the FSM and the correlation coefficients computed with the RM. We can see that the statistics obtained by the RM are consistent with the FSM for almost all nodes. Small errors are detected on the Dirichlet boundaries. In fact, the RM statistics slightly

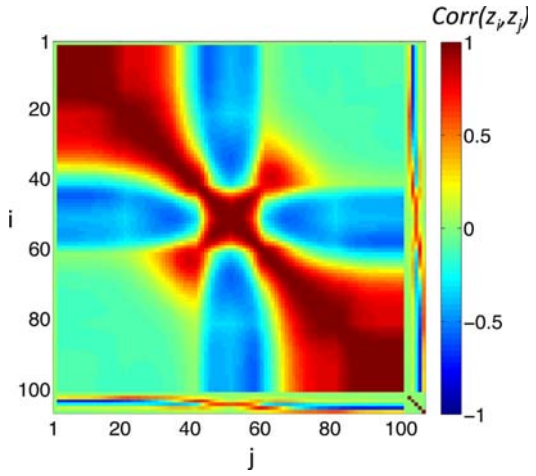

Figure 4. Matrix of the correlation coefficients of the extended state associated with the ensemble of FSM solutions for TC1.

overestimate the correlation coefficients between the nodes in the first and second zones and the hydraulic conductivity of the first zone. We observe similar results for zone 5. This behavior is due to the small drawdown values near the boundary and to the oscillatory nature of the principal components. To avoid large errors, the RM coefficients are computed in such a way as to match the FSM solution at nodes with large drawdown, i.e., in the neighborhood of the pumping well. As a consequence, the RM solution can be less accurate where drawdown is small. However, we note that the errors reported in Figure 5 are relatively small with respect to the true values of the correlation coefficients shown in Figure 4. This implies that the RM can be used to perform MC simulation.

4.2. Two-Dimensional Test Cases, TC2, TC3, and TC4

[47] In this section we investigate the applicability of the RM to a more complex two-dimensional model, developed to simulate the groundwater flow in a confined aquifer located in the Oristano plain, in west-central Sardinia, Italy [*Cau et al.*, 2002; *Siade et al.*, 2012]. The domain of the Oristano aquifer is discretized using 29,197 nodes and 57,888 triangular elements. The comparison between the FSM and the RM is performed on the basis of the results obtained in three synthetic test cases (TC2, TC3, and TC4). In these test cases, we consider a pumping test with a duration of 4 days. There are six pumping wells extracting at a constant rate of $q = 1000$ m^3/d, and zero Dirichlet boundary conditions are imposed. The aquifer, shown in Figure 6, has a constant thickness ($b = 110$ m) and specific storage ($S_s = 10^{-5}$ m^{-1}). Figure 7 shows the zonation patterns used to model the heterogeneous hydraulic conductivity, with 3 zones in TC2, 7 zones in TC3, and 15 zones in TC4. The lower bound and upper bound of the hydraulic conductivities are $K_i^{\min} = 0.1$ m/d and $K_i^{\max} = 20$ m/d in each zone, respectively. The numerical solution of the FSM requires a CPU time of about 45 s for each realization of the hydraulic conductivity. As a consequence, the CPU time required by the MC method with an ensemble size of $n_{\text{ens}} = 1000$ is about 14 h (taking into account the time for the computation of the ensemble statistics). In this situation, the advantage of using the RM for MC simulation is evident. T2 T3 T4 Tables 2–4 compare the CPU times for the FSM and the RM for TC2, TC3, and TC4, respectively. The offline process is performed with a tolerance $\tau_e = 10^{-3}$ m. For TC2 the validation set $\mathcal{K}$ consists of $n_k = 27$ realizations of hydraulic conductivity. Using Algorithm 2, we select snapshots from 13 of these realizations and compute 545 RM solutions, for a total offline CPU time of 890 s. The final number of principal components is $n_{pc} = 28$, and the corresponding RM is solved in 0.25×10^{-2} s (18,000 times faster than the FSM). The MC simulation with the RM requires 15 s which, when added to the offline process, yields a total computational time of 905 s (55 times faster than the FSM).

[48] In TC3, the larger number of random parameters implies a larger variability in the MC solutions. For this reason, we enlarge the set $\mathcal{K}$ for the validation of the RM,

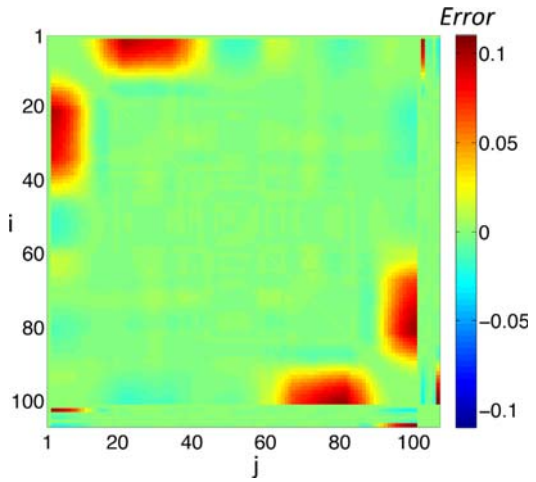

Figure 5. Errors between the correlation coefficients computed with the ensemble associated with the FSM and RM solutions for TC1.

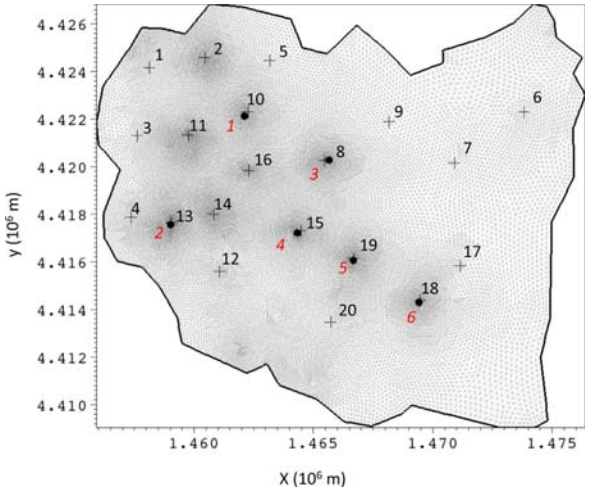

Figure 6. Oristano model with the location of the six pumping wells (dots) and the 20 observation wells (crosses).

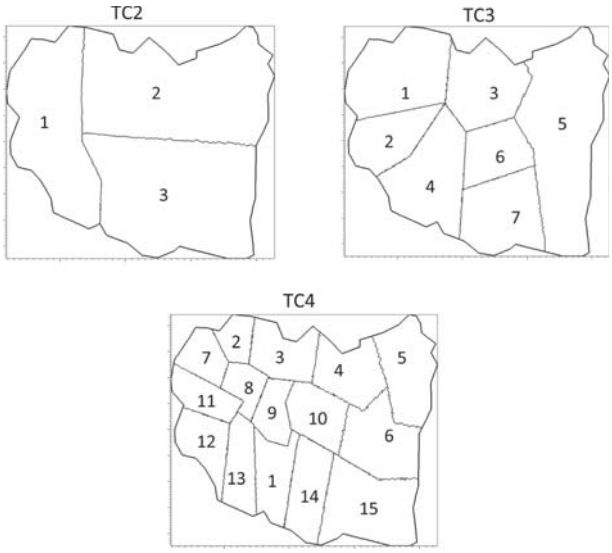

Figure 7. Zonation patterns used for TC2 (three zones), TC3 (seven zones), and TC4 (15 zones) for the Oristano model.

with the consequent offline process that is computationally more expensive than in TC2. Using $n_k = 3^7 = 2187$ combinations of hydraulic conductivity, Algorithm 2 requires 31 FSM solutions and 123,361 RM runs for a total CPU time of 4115 s. The resulting RM consists of 76 principal components and is solved in 0.13×10^{-1} s (3400 times faster than the FSM). The final time for the offline and online processes is 4141 s.

[49] In TC4, the validation of the RM on all 3^{15} combinations of hydraulic conductivity becomes impractical. In this case we apply the offline process directly to the 1000 hydraulic conductivity realizations used in the MC method. Due to the large number of parameters, the offline process requires more FSM runs ($n_{gr} = 65$) than TC3, with a CPU time of 7132 s. The final number of principal components used in the RM is 71 and the total time to apply the MC method is 7158 s.

[50] To verify the accuracy of the final RM on the single realizations, we compute the error $\mathbf{e}(T_F, \hat{\mathbf{k}}^j)$ for all the members of $\mathcal{K}$. Figure 8 shows the head contours at the final simulation time (T_F) obtained with the FSM and RM for the realization with the maximum norm of the error (Figure 8a) and the maximum nodal error (Figure 8b) in TC2. Analogous results have been obtained for TC3 and TC4. For example, in TC2 the realization with the maximum error in the norm (Figure 8a) has hydraulic conductivity values $K_1 = 0.1$ m/d, $K_2 = 10$ m/d, and $K_3 = 0.1$ m/d, while the realization with the maximum nodal error (Figure 8b) has hydraulic conductivity values $K_1 = 20$ m/d, $K_2 = 20$ m/d, and $K_3 = 0.1$ m/d. The results show that, even as the head drastically changes for different combinations of the hydraulic conductivity, the RM solutions compare favorably with the FSM solutions. Similar to the results obtained in the one-dimensional test case, we note that the RM solution is most accurate in the neighborhood of the pumping wells, i.e., in the regions with larger drawdown, while it becomes less accurate near the boundary where the drawdown is small.

[51] Since the RM solutions do not perfectly match the FSM solutions for each realization, we are now interested in evaluating how these errors affect the leading statistical moments of the head that are usually approximated with the MC methods. With this purpose, in Figure 9 we compare the expected value and the variance of the ensemble of the FSM and the RM solutions for TC4. Analogous results have been obtained for TC2 and TC3. The results show that the RM satisfactorily reproduces the mean head field in all test cases. However, errors in the variance are larger and, as expected from the previous results, there is an underestimation of the variance of the head in areas far from the pumping wells.

[52] Finally, we analyze the empirical distribution of head at 20 observation wells indicated in Figure 6. To compare the data obtained with FSM and RM, we apply the two-sample Kolmogorov-Smirnov test (KS) with the null hypothesis that the two ensembles are from the same continuous distribution. The test is performed at several output times (1 min, 5 min, 10 min, 30 min, 1 h, 2 h, 6 h, 12 h, 1 d, 2 d, 3 d, and 4 d). The results obtained indicate that the KS-test fails at the initial times when drawdown is small over the entire domain. Consistent with the previous results, the KS test frequently fails on observations wells that are located closer to the boundary (e.g., wells number 1, 3, and 6). However, most importantly, the null hypothesis is validated at almost all output times for the observation wells that are in the neighborhood of the pumping wells (e.g., well numbers 8, 10, 13, 15, 18, and 19).

Table 2. Comparison Between the FSM and RM CPU Times for the MC Simulation for TC2

			Time for One Iteration (s)	Total Time (s)
FSM	$n_{\text{ens}} = 1{,}000$	$n_{nd} = 29{,}197$	45	50,000
RM online	$n_{\text{ens}} = 1{,}000$	$n_{pc} = 25$	0.25×10^{-2}	15
RM offline	$n_k = 27$	$n_{gr} = 13$		890
RM total				905

Table 3. Comparison Between the FSM and RM CPU Times for the MC Simulation for TC3

			Time for One Iteration (s)	Total Time (s)
FSM	$n_{\text{ens}} = 1{,}000$	$n_{nd} = 29{,}197$	45	50,000
RM online	$n_{\text{ens}} = 1{,}000$	$n_{pc} = 76$	0.13×10^{-1}	26
RM offline	$n_k = 2{,}187$	$n_{gr} = 31$		4,115
RM total				4,141

Table 4. Comparison Between the FSM and RM CPU Times for the MC Simulation for TC4

			Time for One Iteration (s)	Total Time (s)
FSM	$n_{\text{ens}} = 1{,}000$	$n_{nd} = 29{,}197$	45	50,000
RM online	$n_{\text{ens}} = 1{,}000$	$n_{pc} = 71$	10^{-2}	26
RM offline	$n_k = 1{,}000$	$n_{gr} = 65$		7,132
RM total				7,158

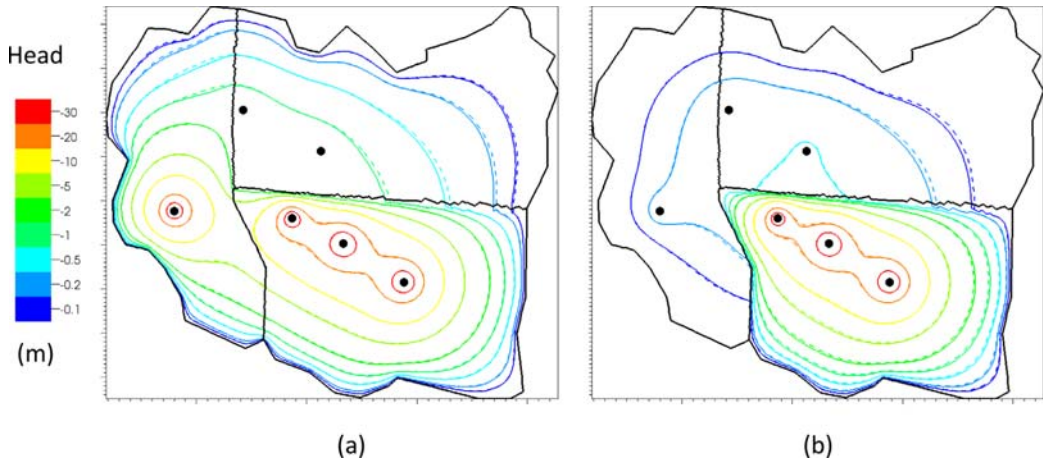

Figure 8. Comparison between the head obtained by solving the FSM (continuous line) and RM (dashed line) for the realizations of the hydraulic conductivity with the (a) maximum norm of the error and (b) maximum nodal error for TC2.

4.3. Offline Algorithm: Dependency on $\mathcal{K}$

[53] In this section we investigate the dependency of the RM accuracy to the validation set $\mathcal{K}$. We consider Algorithm 2 for TC2 with $\mathcal{K}$ given by (i) the complete set of combinations of upper bound, lower bound and the mean of hydraulic conductivity ($n_k = 27$), represented by $\mathcal{K}^{\text{up-low}}$, and (ii) a set of random realizations, denoted by $\mathcal{K}^{\text{MC}}$, of sizes $n_k = 27$, 50, 100, 200, 500, and 1000. To avoid the dependency of the greedy algorithm to the scaled residual, the validation condition is based directly on the norm of the error. The resulting reduced-order models are compared on the basis of the maximum error on the solutions associated with the set $\mathcal{L}$ of 1000 MC realizations of hydraulic conductivity (different from the realizations considered in the offline algorithm). Figure 10 shows these maximum errors obtained for the different choices of $\mathcal{K}$ as a function of the dimension n_k. Moreover, in Figure 10 we highlight the number of principal components obtained after the greedy algorithm. Figure 10 shows that our choice of using $\mathcal{K}^{\text{up-low}}$ in the offline algorithm provides better results than considering $\mathcal{K}^{\text{MC}}$ with $n_k = 27$, 50, and 100 random realizations. However, in TC2, $\mathcal{K}^{\text{up-low}}$ has only 27 realizations and is not sufficient to describe the probability space as accurately as $\mathcal{K}^{\text{MC}}$ with $n_k = 200$, 500, and 1000 realizations. To see if $\mathcal{K}^{\text{up-low}}$ is a reasonable choice for the validation set, we apply the offline algorithm to validate the RM on the set $\mathcal{K} = \mathcal{K}^{\text{up-low}} + \mathcal{K}^{\text{MC}}$ with 1000 random realizations. In this case the greedy algorithm computes the first 22 principal components from eight realizations belonging to $\mathcal{K}^{\text{up-low}}$, achieving a maximum norm of the error of 0.003 m on the entire $\mathcal{K}$. Only the last two principal components are computed from the realizations in $\mathcal{K}^{\text{MC}}$. Figure 11 shows that the RM validated on the set $\mathcal{K} = \mathcal{K}^{\text{up-low}} + \mathcal{K}^{\text{MC}}$ also maintains the desired accuracy (errors smaller than the threshold τ_e) when applied to the independent set $\mathcal{L}$.

4.4. Offline Algorithm: Scaled Residual

[54] In this section we show the practical advantages of using the scaled residual for the estimation of the errors in

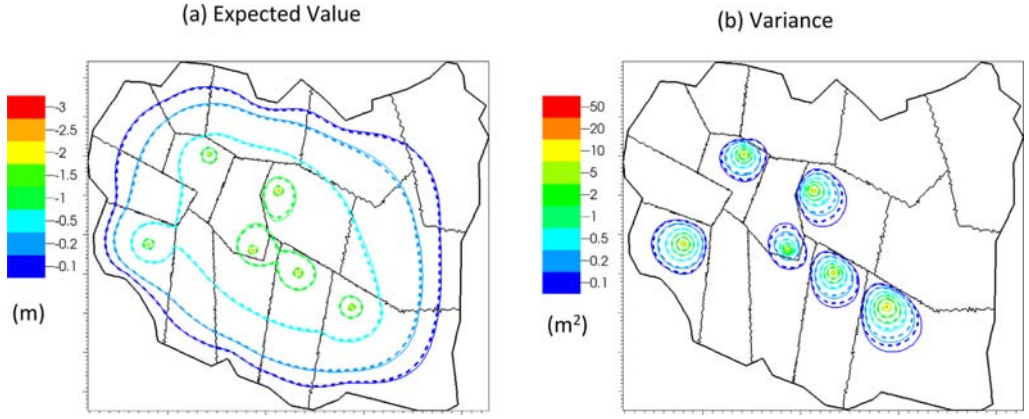

Figure 9. (a) Expected value and (b) variance of the ensemble of the drawdown obtained with the FSM (continuous lines) and the RM (dashed lines) results for TC4.

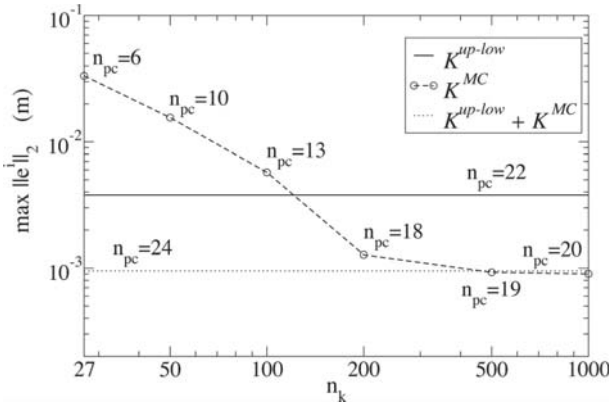

Figure 10. Maximum error of the RM on 1000 MC realizations, for different choices of the validation set $\mathcal{K}$ in TC2. The horizontal line represents the error associated with $\mathcal{K} = \mathcal{K}^{\text{up-low}}$ (continuous line) and $\mathcal{K} = \mathcal{K}^{\text{up-low}} + \mathcal{K}^{\text{MC}}$ (dotted line). The dashed line shows the errors associated with $\mathcal{K} = \mathcal{K}^{\text{MC}}$, with $n_k = 27$, 50, 100, 200, 500, and 1000.

the greedy algorithm. We consider Algorithm 2 in TC2 with the validation set $\mathcal{K} = \mathcal{K}^{\text{up-low}}$. The estimation of the error is performed with (a) the scaled norm of the residual $\hat{R}^i$ and (b) the norm of the residual R^i. Figure 11 shows the main results of the application of these two greedy algorithms, comparing the maximum error with its estimation as a function of the number of the principal components. In both cases, the maximum error falls under the threshold value τ_e after six iterations of the greedy algorithm, with 20 principal components. Using the scaled norm of the residual $\hat{R}^i$ (Figure 11a), the error is underestimated in the first iterations due to the lack of information for interpolating the scaling factors. However, in the subsequent iterations, we obtain a good estimation of the error and the greedy algorithm stops with only five additional iterations. Instead, estimating the error with the residual R^i (Figure 11b) shows an overestimation of the error. As consequence, a larger number of iterations of the greedy algorithm are performed, with unnecessary computation of additional FSM solutions and principal components.

5. Summary and Conclusions

[55] We have presented a model-order reduction technique that addresses the computational burden associated with the MC simulations of confined groundwater flow models with stochastic hydraulic conductivity. We proposed a new offline algorithm (Algorithm 2) for the computation of parameter-independent principal components, which constitutes the core of the RM. In this offline process we combined a residual-based greedy algorithm for the selection of snapshots in the parameter space with a quasi-optimal method for the selection of snapshots in time. The algorithm starts with an initial set of principal components and improves this set until the RM solution is validated on an appropriately chosen set $\mathcal{K}$ of hydraulic conductivity realizations. The validation condition is provided by estimating the error norm with the norm of the residual scaled by a suitable coefficient (equations (16) and (17)). The greedy algorithm selects the new snapshots corresponding to the hydraulic conductivity value that maximizes the estimation of the RM error (equation (18)). Then, the FSM solution is used for the selection of the snapshots at the optimal times given by equation (13). Finally, the principal component analysis performed on the set of snapshots produces the new principal components needed to improve the RM solution. This new methodology allows the evaluation of the reduced model with only a few essential FSM runs, ensuring the computational efficiency of the algorithm and the accuracy of the RM solution. Once the principal components are computed, the application of the RM to the MC simulation is straightforward. Since the RM is parameter independent, it can be used efficiently to compute the main statistics associated

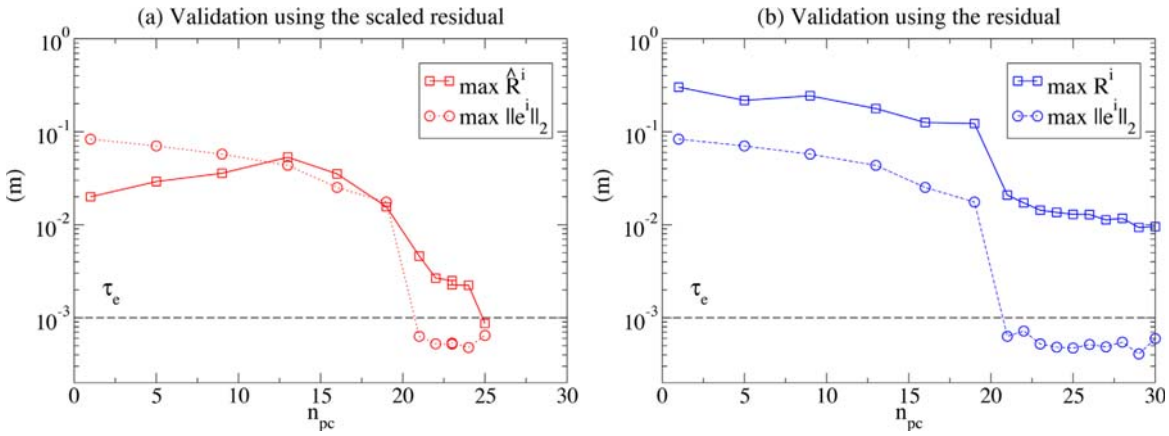

Figure 11. Comparison between the estimation of the error at each iteration of the greedy algorithm using the validation condition on (a) the maximum-scaled norm of the residual $\hat{R}^i$ and (b) the maximum norm of the residual R^i. The dotted line shows the maximum norm of the error, while the horizontal dashed line is the threshold value τ_e for the termination of the greedy algorithm.

with the ensemble of solutions, such as the expected value and the covariance of the head.

[56] We first verified our methodology on a one-dimensional test case with five conductivity zones (TC1) and then applied it to a two-dimensional model of the Oristano aquifer with 3, 7, and 15 different conductivity zones (TC2, TC3, and TC4). The RM solution was compared with the classical MC solution in terms of CPU times, expected head values, and head variance in the entire domain as well as the empirical probability distribution function of the head at the observation wells. The numerical results lead to the following conclusions.

[57] Our algorithm reduced the 29,197 nodes of the Oristano model to less than 100 principal components, with a corresponding RM solution that is at least 1000 times faster than the FSM solution. The computation of the principal components in the offline process is the most expensive part of the procedure, as it requires a certain number of FSM solutions. The number of FSM runs used by our offline process is reduced by using the scaled residual to estimate the error norm driving the greedy algorithm. This number increased with the number of random parameters, due to the fact that the FSM solutions corresponding to larger parameter sets have more degrees of freedom and, as a consequence, the RM needs more information to accurately describe the space of the solutions. Nevertheless, the numerical results demonstrate that, with 15 zones, our methodology (offline plus online) is more than 10 times faster than the standard MC approach with the same level of accuracy. However, we would like to note that our ultimate goal is to develop a parameter-independent RM that can be used for fast online execution. This goal has been achieved, as demonstrated by an application of the proposed methodology to the Oristano aquifer in Italy, where the FSM was reduced by 3 orders of magnitude and ran 1000 times faster than the FSM. Moreover, our offline algorithm allows the construction of the RM with a limited number of FSM, rendering the proposed scheme attractive for large-scale computations.

[58] The comparison between the statistics of the ensemble of solutions given by the RM and FSM suggests that our RM produces the correct expected value of the head over the entire domain, while it slightly underestimates the variance in the regions of small drawdown. In addition, the two-sided KS test applied to the empirical distributions of the heads at the observation wells indicates that the RM is most accurate in the neighborhood of the pumping wells, i.e., where the response of the system to pumping is higher. We attribute this fact to the methodology that we employed for the generation of principal components. In fact, with the principal component analysis, we keep the principal components corresponding to the larger eigenvalues that describe the dominating characteristics of the solution, while we discard the principal components corresponding to small eigenvalues, which are only useful for a detailed description of the solution in regions of low variance, i.e., regions with low sensitivity to pumping.

[59] Further research is needed to extend our methodology to compute the principal components for the case of spatially distributed random hydraulic conductivities, particularly for aquifers with strong local heterogeneity, for which the interpolation scheme employed to evaluate the scaling factors used in Algorithm 2 needs to be completely revised. How to derive reduced models under such situations is a topic of future research.

Appendix A: Algorithm 1: RM Initialization

1) Compute T_s for $\hat{\mathbf{k}}^1$
2) Compute $\hat{t}_1, \ldots, \hat{t}_{n_{sn}}$
3) Solve equation (4) and store $\mathbf{s}_{\hat{t}_1}, \ldots, \mathbf{s}_{\hat{t}_{n_{sn}}}$
4) Compute $\mathbf{p}_1^1, \ldots, \mathbf{p}_{n_{sn}}^1$
5) $n_{pc} \leftarrow 1$
6) $\mathbf{P} \leftarrow \{\mathbf{p}_1^1\}$
7) Solve equation (6) for $\hat{\mathbf{k}}^1$
8) Compute $\|\mathbf{e}(T_F, \hat{\mathbf{k}}^1)\|_2$
9) **While** $\|\mathbf{e}(T_F, \hat{\mathbf{k}}^1)\|_2 \geq \tau_e$
   a) $n_{pc} \leftarrow n_{pc} + 1$
   b) $\mathbf{P} \leftarrow \{\mathbf{p}_1^1, \ldots, \mathbf{p}_{n_{pc}}^1\}$
   c) Solve equation (6) for $\mathbf{k}^1$
   d) Compute $\|\mathbf{e}(T_F, \hat{\mathbf{k}}^1)\|_2$
10) **End While**

Appendix B: Algorithm 2: Offline: Modified Greedy Algorithm

a) $n_{gr} \leftarrow 0$
b) $n_{pc} \leftarrow 0$
c) $\hat{\mathbf{k}}^{*1} \leftarrow \hat{\mathbf{k}}^1$
d) $\hat{R}(T_F, \hat{\mathbf{k}}^{*1}) \leftarrow 2\tau_e$
e) **While** $\hat{R}(T_F, \hat{\mathbf{k}}^{*n_{gr}+1}) \geq \tau_e$
   (1) $n_{gr} \leftarrow n_{gr} + 1$
   (2) Compute $\mathbf{p}_1^{*n_{gr}}, \ldots, \mathbf{p}_{n_{sn}}^{*n_{gr}}$ from $\hat{\mathbf{k}}^{*n_{gr}}$ (Algorithm 1)
   (3) $i \leftarrow n_{gr}$
   (4) **While** $\hat{R}(T_F, \hat{\mathbf{k}}^{*i}) \geq \tau_e$
      a. $n_{pc} \leftarrow n_{pc} + 1$
      b. Improve $\mathbf{P}$ with a principal component from $\hat{\mathbf{k}}^{*i}$
      c. **For** $j = 1 \rightarrow n_{gr}$ **(**Loop on $\mathcal{K}^*$)
         i. Solve the RM equation (6) for $\hat{\mathbf{k}}^{*j}$
         ii. Compute $\|\mathbf{e}(T_F, \hat{\mathbf{k}}^{*j})\|_2$, $\hat{R}(T_F, \hat{\mathbf{k}}^{*j})$ and ρ^{*j} (equation (15))
      d. **End For**
      e. $i = \arg\max_{j=1,\ldots,n_{gr}} \hat{R}(T_F, \mathbf{k}^{*j})$
   (5) **End While**
   (6) **For** $j = 1 \rightarrow n_k$ **(**Loop on $\mathcal{K}$)
      a. Solve the RM equation (6) for $\hat{\mathbf{k}}^j$
      b. Compute ρ^j (equation (16)) and $\hat{R}(T_F, \hat{\mathbf{k}}^j)$ (equation (17))
   (7) **End For**
   (8) $\hat{\mathbf{k}}^{*n_{gr}+1} = \arg\max_{\hat{\mathbf{k}} \in \mathbf{K}} \hat{R}(T_F, \hat{\mathbf{k}}^j)$
f) **End While**

[60] **Acknowledgments.** This material is based on work partially supported by NSF under award EAR-0910507, ARO under award W911NF-10-1-0124, and an AECOM endowment. We also acknowledge the financial support of the European Commission (grant FP7-ENV-2009-1-244151), the CARIPARO Foundation (grant "NPDE-Nonlinear Partial Differential Equations: Models, Analysis, and Control-Theoretic Problems"), the "Ing. Aldo Gini" Foundation and the University of Padua (grant STPD08RWBY). We thank three anonymous reviewers for their in-depth and constructive reviews.

References

Baú, D. A. (2012), Planning of groundwater supply systems subject to uncertainty using stochastic flow reduced models and multi-objective evolutionary optimization, *Water Resour. Manage.*, *26*(9), 2513–2536, doi:10.1007/s11269-012-0030-4.

Bear, J. (1979), *Hydraulics of Groundwater*, McGraw-Hill, New York.

Cau, P. L., G. Lecca, M. Putti, and C. Paniconi (2002), The influence of a confining layer on saltwater intrusion and surface recharge and groundwater extraction conditions, in *Computational Methods in Water Resources, Dev. in Water Resour.*, vol. 1, edited by S. M. Hassanizadeh et al., pp. 493–500, Elsevier, Amsterdam.

Chen, Y., and D. Zhang (2006), Data assimilation for transient flow in geologic formations via ensemble Kalman filter, *Adv. Water Resour.*, *29*(8), 1107–1122, doi:10.1016/j.advwatres.2005.09.007.

Dagan, G. (1982), Stochastic modeling of groundwater flow by unconditional and conditional probabilities: 1. Conditional simulation and the direct problem, *Water Resour. Res.*, *18*(4), 813–833, doi:10.1029/WR018i004p00813.

Gambolati, G., M. Putti, and C. Paniconi (1999), Three-dimensional model of coupled density-dependent flow and miscible salt transport in groundwater, in *Seawater Intrusion in Coastal Aquifers: Concepts, Methods, and Practices*, edited by J. Bear et al., pp. 315–362, Kluwer Acad., Dordrecht, Netherlands.

Ghanem, R. and P. Spanos (1991), *Stochastic Finite Elements: A Spectral Approach*, Springer-Verlag, New York.

Grepl, M. A., and A. T. Patera (2005), A posteriori error bounds for reduced-basis approximations of parametrized parabolic partial differential equations, *ESAIM-Math. Model. Numer. Anal*, *39*(1), 157–181, doi:10.1051/m2an:2005006.

Guadagnini, A., and S. P. Neuman (1999), Nonlocal and localized analyses of conditional mean steady state flow in bounded, randomly nonuniform domains: 1. Theory and computational approach, *Water. Resour. Res.*, *35*(10), 2999–3018, doi:10.1029/1999WR900160.

Haasdonk, B., and M. Ohlberger (2011), Efficient reduced models and a-posteriori error estimation for parametrized dynamical systems by offline/online decomposition, *Math. Comput. Model. Dyn.*, *17*(2), 145–161, doi:10.1080/13873954.2010.514703.

Hasenauer, J., M. Löhning, M. Khammash, and F. Allgöwer (2012), Dynamical optimization using reduced order models: A method to guarantee performance, *J. Process Contr.*, *22*(8), 1490–1501, doi:10.1016/j.jprocont.2012.01.017.

Hendricks Franssen, H. J., A. Alcolea, M. Riva, M. Bakr, N. van der Wiel, F. Stauffer, and A. Guadagnini (2009), A comparison of seven methods for the inverse modelling of groundwater flow. Application to the characterisation of well catchments, *Adv Water Resour.*, *32*(6), 851–872, doi:10.1016/j.advwatres.2009.02.011.

Hinze, M., and M. Kunkei (2012), Residual based sampling in POD model order reduction of drift-diffusion equations in parameterized electrical networks, ZAMM-Z. *Angew. Math. Mech.*, *92*(2), 91–104, doi:10.1002/zamm.201100004.

Kunisch, K., and S. Volkwein (2001), Galerkin proper orthogonal decomposition methods for parabolic problems, *Numer. Math.*, *148*(1), 117–148, doi:10.1007/s002110100282.

Li, H., and D. Zhang (2007), Probabilistic collocation method for flow in porous media: Comparisons with other stochastic methods, *Water Resour. Res.*, *43*, W09409, doi:10.1029/2006WR005673.

McPhee, J., and W. W.-G. Yeh (2008), Groundwater management using model reduction via empirical orthogonal functions, *J. Water Resour. Plann. Manage.*, *134*(2), 161–170, doi:10.1061/(ASCE)0733–9496(2008)134:2(161).

Oliver, D. S., and Y. Chen (2011), Recent progress on reservoir history matching: A review, *Comput. Geophys.*, *15*(1), 185–221, doi:10.1007/s10596-010-9194-2.

Pasetto, D., A. Guadagnini, and M. Putti (2011), POD-based Monte Carlo approach for the solution of regional scale groundwater flow driven by randomly distributed recharge, *Adv. Water Resour.*, *34*(11), 1450–1463, doi:10.1016/j.advwatres.2011.07.003.

Pasetto, D., M. Camporese, and M. Putti (2012), Ensemble Kalman filter versus particle filter for a physically-based coupled surface-subsurface model, *Adv. Water Resour.*, *47*, 1–13, doi:10.1016/j.advwatres.2012.06.009.

Robert, C., and G. Casella (2010), *Monte Carlo Statistical Methods*, Springer, New York.

Rovas, D. V., L. Machiels, and Y. Maday (2006), Reduced-basis output bound methods for parabolic problems, *IMA J. Numer. Anal.*, *26*(3), 423–445, doi:10.1093/imanum/dri044.

Siade, A. J., M. Putti, and W. W.-G. Yeh (2010), Snapshot selection for groundwater model reduction using proper orthogonal decomposition, *Water Resour. Res.*, *46*, W08539, doi:10.1029/2009WR008792.

Siade, A. J., M. Putti, and W. W.-G. Yeh (2012), Reduced order parameter estimation using quasilinearization and quadratic programming, *Water Resour. Res.*, *48*, W06502, doi:10.1029/2011WR011471.

Vermeulen, P. T. M., A. W. Heemink, and C. B. M. T. Stroet (2004), Reduced models for linear groundwater flow models using empirical orthogonal functions, *Adv. Water Resour.*, *27*(1), 57–69, doi:10.1016/j.advwatres.2003.09.008.

Yeh, W. W.-G. (1986), Review of parameter identification procedures in groundwater hydrology: The inverse problem, *Water Resour. Res.*, *22*(2), 95–108, doi:10.1029/WR022i002p00095.

Zhang D. X., L. S. Shi, H. B. Chang, and J. Z. Yang (2010), A comparative study of numerical approaches to risk assessment of contaminant transport, *Stochastic Environ. Res. Risk. A.*, *24*(7), 971–84, doi:10.1007/s00477-010-0400-5.